

State-Augmented Learnable Algorithms for Resource Management in Wireless Networks

Navid NaderiAlizadeh, Mark Eisen, and Alejandro Ribeiro

Abstract—We consider resource management problems in multi-user wireless networks, which can be cast as optimizing a network-wide utility function, subject to constraints on the long-term average performance of users across the network. We propose a state-augmented algorithm for solving the aforementioned radio resource management (RRM) problems, where, alongside the instantaneous network state, the RRM policy takes as input the set of dual variables corresponding to the constraints, which evolve depending on how much the constraints are violated during execution. We theoretically show that the proposed state-augmented algorithm leads to feasible and near-optimal RRM decisions. Moreover, focusing on the problem of wireless power control using graph neural network (GNN) parameterizations, we demonstrate the superiority of the proposed RRM algorithm over baseline methods across a suite of numerical experiments.

Index Terms—Radio resource management, wireless networks, graph neural networks, Lagrangian duality, state augmentation, wireless power control.

I. INTRODUCTION

With the proliferation of 5G network implementations across the globe and research already underway for future 6G wireless networks, novel wireless services and capabilities are expected to emerge that require carefully-optimized management of wireless resources. Aside from traditional approaches for addressing such radio resource management (RRM) problems [1]–[5], learning-based methods have recently gained significant traction and demonstrated superior performance over prior approaches [6]–[11]. Such methods are envisioned to play a key role in current and future wireless networks with the ubiquitous availability of computational resources both at the end-user devices and within the network infrastructure [12]–[15].

As a general formulation of the RRM problem, similarly to prior work [6], [9], [16], [17], we consider a network utility maximization problem, subject to multiple constraints, where both the utility and the constraints are defined based on the long-term average performance of users across the network. A common method for solving such problems is to move to the Lagrangian dual domain, where a single objective, i.e., the Lagrangian, can be maximized over the primal variables and minimized over the dual variables, with each dual variable corresponding to a constraint in the original RRM problem. It can be shown that under mild conditions, such problems have null duality gap, hence allowing the use of primal-dual

methods to derive optimal solutions. Even with the introduction of parameterizations for the RRM policy, the duality gap remains small in case of near-universal parameterizations, such as fully-connected deep neural networks. Nevertheless, such primal-dual algorithms lack feasibility guarantees. More precisely, it is unclear whether they lead to RRM decisions that satisfy the constraints in the original RRM problem.

In this paper, we propose an alternative approach to solve the aforementioned constrained RRM problem. In particular, we leverage the fact that dual variables in constrained optimization provide indication of how much the corresponding constraints have been violated or satisfied over time. Using this observation, we incorporate the notion of *state augmentation* from [18], in which the standard wireless network state is augmented with dual variables at each time instance to use as dynamic inputs to the RRM policy. By incorporating dual variables as an augmented input for the RRM policy, we are able to train the policy to adapt its decisions to not only instantaneous channel states, but also to such indications of constraint satisfaction. We establish theoretically how the proposed *state-augmented* RRM algorithm in fact leads to a trajectory of RRM decisions that, unlike in standard primal-dual training methods, are both *feasible*, i.e., satisfy the constraints almost-surely, and *near-optimal*, in the sense that the expected resulting network utility is within a constant additive gap of the optimum.

As a prominent use case of the aforementioned state-augmented algorithm for solving RRM problems, we consider the problem of power control in multi-user interference channels, where the goal is to maximize the network sum-rate, subject to per-user minimum-rate requirements. We model the network state as the set of channel gains at each time step, and use a graph neural network (GNN) parameterization for the RRM policy, that takes as input both the network state and the dual variables at each time step, and outputs the transmit power levels. Through numerical experiments, we show that our proposed state-augmented algorithm, while slightly sacrificing the average performance, significantly outperforms baseline methods in terms of the worst-case user rates, thanks to satisfying the per-user minimum-rate constraints. We also show the benefits of the GNN-based parameterization of the RRM policy in terms of scalability to larger configurations and transferability to unseen network sizes, confirming the findings of prior work using such permutation-equivariant parameterizations [9], [10], [17], [19]–[27].

The rest of the paper is organized as follows. We begin in Section II by formulating the radio resource management problem, in which instantaneous resource allocation decisions

N. NaderiAlizadeh and A. Ribeiro are with the Department of Electrical and Systems Engineering, University of Pennsylvania, Philadelphia, PA 19104, USA (e-mails: {nnaderi, aribeiro}@seas.upenn.edu). M. Eisen is with Intel Labs, Intel Corporation, Hillsboro, OR 97124, USA (e-mail: mark.eisen@intel.com).

are made in response to network states to both maximize a utility and satisfy constraints on the long-term network performance. In Section III, we show how parameterized RRM policies, trained via gradient-based methods, can lead to feasible RRM decisions that are optimal to within a constant additive gap by solving the problem in the Lagrangian dual domain. Such an algorithm is practically limited, however, due to, among other things, the large computational expense required during inference.

In Section IV, we describe our proposed approach of using state augmentation to learn alternative algorithms for RRM training and inference. We further prove its feasibility and near-optimality properties under proper assumptions on the expressive power of the state-augmented policy. In Section V, we show the application of the proposed method to power control problems in multi-user interference channels with graph neural network parameterizations through an extensive series of numerical simulations. Finally, we conclude the paper in Section VI.

II. PROBLEM FORMULATION

We consider a wireless network operating over a series of time steps $t \in \{0, 1, 2, \dots, T-1\}$, where at each time step t , the set of channel gains in the network, or the *network state*, is denoted by $\mathbf{H}_t \in \mathcal{H}$. Given the network state, we let $\mathbf{p}(\mathbf{H}_t)$ denote the vector of *radio resource management (RRM)* decisions across the network, where $\mathbf{p} : \mathcal{H} \rightarrow \mathbb{R}^a$ denotes the RRM function. These RRM decisions subsequently lead to the network-wide performance vector $\mathbf{f}(\mathbf{H}_t, \mathbf{p}(\mathbf{H}_t)) \in \mathbb{R}^b$, with $\mathbf{f} : \mathcal{H} \times \mathbb{R}^a \rightarrow \mathbb{R}^b$ denoting the performance function.

Given a concave utility $\mathcal{U} : \mathbb{R}^b \rightarrow \mathbb{R}$ and a set of c concave constraints $\mathbf{g} : \mathbb{R}^b \rightarrow \mathbb{R}^c$, we define the generic RRM problem as

$$\max_{\{\mathbf{p}(\mathbf{H}_t)\}_{t=0}^{T-1}} \mathcal{U} \left(\frac{1}{T} \sum_{t=0}^{T-1} \mathbf{f}(\mathbf{H}_t, \mathbf{p}(\mathbf{H}_t)) \right), \quad (1a)$$

$$\text{s.t.} \quad \mathbf{g} \left(\frac{1}{T} \sum_{t=0}^{T-1} \mathbf{f}(\mathbf{H}_t, \mathbf{p}(\mathbf{H}_t)) \right) \geq \mathbf{0}, \quad (1b)$$

where the objective and the constraints are derived based on the *ergodic average* network performance $\frac{1}{T} \sum_{t=0}^{T-1} \mathbf{f}(\mathbf{H}_t, \mathbf{p}(\mathbf{H}_t))$ rather than the instantaneous performance. The goal of the RRM problem is, therefore, to derive the optimal vector of RRM decisions $\mathbf{p}(\mathbf{H}_t)$ for any given network state $\mathbf{H}_t \in \mathcal{H}$.

III. PARAMETERIZED GRADIENT-BASED RRM ALGORITHMS IN THE DUAL DOMAIN

As (1a) shows, problem (1) entails an infinite-dimensional search over the set of RRM decisions $\mathbf{p}(\mathbf{H})$ for any given network state \mathbf{H} , which is practically infeasible. Therefore, we resort to *parameterizing* the RRM policy and replacing $\mathbf{p}(\mathbf{H})$ with $\mathbf{p}^\theta(\mathbf{H}; \theta)$, where $\theta \in \Theta$ denotes a finite-dimensional set

of parameters. This, in turn, leads to the *parameterized* RRM problem

$$P^* = \max_{\theta \in \Theta} \mathcal{U} \left(\frac{1}{T} \sum_{t=0}^{T-1} \mathbf{f}(\mathbf{H}_t, \mathbf{p}^\theta(\mathbf{H}_t; \theta)) \right), \quad (2a)$$

$$\text{s.t.} \quad \mathbf{g} \left(\frac{1}{T} \sum_{t=0}^{T-1} \mathbf{f}(\mathbf{H}_t, \mathbf{p}^\theta(\mathbf{H}_t; \theta)) \right) \geq \mathbf{0}, \quad (2b)$$

where the maximization is now performed over the set of parameters $\theta \in \Theta$.

In order to solve problem (2), we move to the Lagrangian dual domain. To derive the Lagrangian dual problem, we first introduce the Lagrangian function, with non-negative dual multipliers $\mu \in \mathbb{R}_+^c$ associated with the constraints in (2b), as

$$\mathcal{L}(\theta, \mu) = \mathcal{U} \left(\frac{1}{T} \sum_{t=0}^{T-1} \mathbf{f}(\mathbf{H}_t, \mathbf{p}^\theta(\mathbf{H}_t; \theta)) \right) + \mu^T \mathbf{g} \left(\frac{1}{T} \sum_{t=0}^{T-1} \mathbf{f}(\mathbf{H}_t, \mathbf{p}^\theta(\mathbf{H}_t; \theta)) \right). \quad (3)$$

The Lagrangian in (3) can be optimized using gradient-based methods. In particular, we seek to maximize over θ , while subsequently minimizing over the dual multipliers μ , i.e.,

$$D^* := \min_{\mu \in \mathbb{R}_+^c} \max_{\theta \in \Theta} \mathcal{L}(\theta, \mu). \quad (4)$$

To train the model parameters θ , we introduce an *iteration* duration T_0 , which we define as the number of time steps between consecutive model parameter updates. Based on this notion, we define an iteration index $k \in \{0, 1, 2, \dots, K-1\}$ with $K = \lfloor T/T_0 \rfloor$, where the model parameters are updated as

$$\theta_k = \arg \max_{\theta \in \Theta} \left[\mathcal{U} \left(\frac{1}{T_0} \sum_{t=kT_0}^{(k+1)T_0-1} \mathbf{f}(\mathbf{H}_t, \mathbf{p}^\theta(\mathbf{H}_t; \theta)) \right) + \mu_k^T \mathbf{g} \left(\frac{1}{T_0} \sum_{t=kT_0}^{(k+1)T_0-1} \mathbf{f}(\mathbf{H}_t, \mathbf{p}^\theta(\mathbf{H}_t; \theta)) \right) \right], \quad (5)$$

while the dual variables are updated recursively as

$$\mu_{k+1} = \left[\mu_k - \eta_\mu \mathbf{g} \left(\frac{1}{T_0} \sum_{t=kT_0}^{(k+1)T_0-1} \mathbf{f}(\mathbf{H}_t, \mathbf{p}^\theta(\mathbf{H}_t; \theta_k)) \right) \right]_+, \quad (6)$$

where $[\cdot]_+$ denotes projection onto the non-negative orthant, i.e., $[\cdot]_+ := \max(\cdot, 0)$, and η_μ denotes the learning rate corresponding to the dual variables μ .

Given the aforementioned training procedure, we can establish the following result on the generated RRM decisions.

Theorem 1. *Consider a RRM algorithm, in which the primal parameters θ and the dual variables μ follow the dynamics in (5) and (6), respectively. Assuming that*

- *there exists a positive constant $G > 0$ such that for any channel gain matrix \mathbf{H} and any vector of RRM decisions $\hat{\mathbf{p}}$, we have $|g_i(\mathbf{f}(\mathbf{H}, \hat{\mathbf{p}}))| \leq G, \forall i \in \{1, \dots, c\}$; and,*

- there exists a strictly-feasible set of model parameters $\hat{\theta}$ such that $\mathbf{g}\left(\frac{1}{T}\sum_{t=0}^{T-1}\mathbf{f}(\mathbf{H}_t, \mathbf{p}^\theta(\mathbf{H}_t; \hat{\theta}))\right) \geq G'\mathbf{1}$ for some positive constant $G' > 0$,

then the resulting RRM decisions satisfy the desired constraints, i.e.,

$$\lim_{T \rightarrow \infty} \mathbf{g}\left(\frac{1}{T}\sum_{t=0}^{T-1}\mathbf{f}(\mathbf{H}_t, \mathbf{p}^\theta(\mathbf{H}_t; \theta_{\lfloor t/T_0 \rfloor}))\right) \geq \mathbf{0}, \quad a.s. \quad (7)$$

and they are within a constant additive gap of the optimum, i.e.,

$$\lim_{T \rightarrow \infty} \mathbb{E}\left[\mathcal{U}\left(\frac{1}{T}\sum_{t=0}^{T-1}\mathbf{f}(\mathbf{H}_t, \mathbf{p}^\theta(\mathbf{H}_t; \theta_{\lfloor t/T_0 \rfloor}))\right)\right] \geq P^* - \frac{c\eta\mu G^2}{2}. \quad (8)$$

Proof. See Appendix A. \square

Theorem 1 shows that the resulting RRM algorithm is both feasible and near-optimal if it is run for a large-enough number of time steps. This is notable, as with regular primal-dual methods, the RRM policies are not guaranteed to lead to a feasible set of RRM decisions, while such a feasibility guarantee exists for the RRM algorithm in (5)-(6). Note that the main factor that distinguishes (5)-(6) from regular primal-dual methods (see, e.g., [6]) is the maximization step in (5), which adapts the RRM policy parameters to the dual variables at each iteration.

Nevertheless, the iterative RRM algorithm in (5)-(6) presents a set of challenges that make it unsuitable for use in practice. First, maximizing the Lagrangian in (5) requires non-causal knowledge of the network states in the future (see the definition of the Lagrangian in (3)), which is impossible to obtain during execution, even though it might be viable during the training phase. Second, as Theorem 1 demonstrates, convergence to feasible and near-optimal RRM performance is only obtained as operation time T tends to infinity. Thus, training iterations cannot be stopped at a finite time step, as there may not exist an iteration index k for which θ_k (or alternatively, a time average of $\{\theta_{k'}\}_{k'=0}^{k-1}$) is optimal or feasible. Finally, in the maximization problem in (5), the optimal set of model parameters needs to be found at each time step for a different vector of dual variables μ_k , which can be computationally expensive, especially during the execution phase. This underscores the need to construct an algorithm that does not require memorization of the model parameters θ for any given set of dual variables μ , which we discuss next.

IV. PROPOSED STATE-AUGMENTED RRM ALGORITHM

In light of the aforementioned challenges, we propose a *state-augmented* RRM algorithm, similarly to [18], where the network state \mathbf{H}_t at each time step t is augmented by the corresponding set of dual variables $\mu_{\lfloor t/T_0 \rfloor}$, which are simultaneously used as inputs to the RRM policy. In particular, we introduce an alternative parameterization for the RRM policy, in which we represent the RRM decisions $\mathbf{p}(\mathbf{H})$ using the parameterization $\mathbf{p}^\phi(\mathbf{H}, \mu; \phi)$, where $\phi \in \Phi$ denotes the set of parameters of the state-augmented RRM policy.

For a set of dual variables $\mu \in \mathbb{R}_+^c$, we define the *augmented* Lagrangian as

$$\mathcal{L}_\mu(\phi) = \mathcal{U}\left(\frac{1}{T}\sum_{t=0}^{T-1}\mathbf{f}(\mathbf{H}_t, \mathbf{p}^\phi(\mathbf{H}_t, \mu; \phi))\right) + \mu^T \mathbf{g}\left(\frac{1}{T}\sum_{t=0}^{T-1}\mathbf{f}(\mathbf{H}_t, \mathbf{p}^\phi(\mathbf{H}_t, \mu; \phi))\right). \quad (9)$$

Then, considering a probability distribution p_μ for the dual variables, we define the optimal state-augmented RRM policy as that which maximizes the expected augmented Lagrangian over the distribution of all dual parameters, i.e.,

$$\phi^* = \arg \max_{\phi \in \Phi} \mathbb{E}_{\mu \sim p_\mu} [\mathcal{L}_\mu(\phi)]. \quad (10)$$

Utilizing the state-augmented policy parameterized by ϕ^* in (10), we can obtain the Lagrangian-maximizing RRM decision $\mathbf{p}(\mathbf{H}, \mu; \phi)$ for each dual iterate $\mu = \mu_k$. We therefore substitute the two-step update sequence in (5)-(6) with the state-augmented version of the dual multiplier update, i.e.,

$$\mu_{k+1} = \left[\mu_k - \eta_\mu \mathbf{g}\left(\frac{1}{T_0} \sum_{t=kT_0}^{(k+1)T_0-1} \mathbf{f}(\mathbf{H}_t, \mathbf{p}^\phi(\mathbf{H}_t, \mu_k; \phi^*))\right) \right]_+. \quad (11)$$

Note in (11) the usage of the state-augmented RRM policy $\mathbf{p}^\phi(\mathbf{H}_t, \mu_k; \phi^*)$ under the current dual multiplier at iteration k . Thus, in solving for the optimal state-augmented policy in (10), we are effectively *learning* a parameterized model that, in conjunction with (11), executes the dual descent method in (5)-(6).

Indeed, the main reason that we consider the state-augmented parameterization $\mathbf{p}(\mathbf{H}, \mu; \phi)$ is to resolve the challenge of memorizing the model parameters for any given set of dual variables. This implies that we need parameterizations with enough expressive power so that the RRM decisions made via the set of parameters ϕ^* in (10) can closely approximate the ones using the iterative model parameters $\{\theta_k(\mu_k)\}_{k=0}^{K-1}$ in (5), where we have made explicit the dependence of θ_k on μ_k , $\forall k \in \{0, 1, 2, \dots, K-1\}$. To that end, we focus on a specific class of parameterizations, referred to as *near-universal* parameterizations, which we define next.

Definition 1. Consider arbitrary functions $\theta : \mathbb{R}_+^c \rightarrow \Theta$ and $\mathbf{p}^\theta : \mathcal{H} \times \Theta \rightarrow \mathbb{R}^a$. A parameterization $\mathbf{p}^\phi(\mathbf{H}, \mu; \phi)$ with $\phi \in \Phi$ is *near-universal* with degree $\epsilon > 0$ for functions $\mathbf{p}^\theta(\mathbf{H}; \theta(\mu))$ if for any network state $\mathbf{H} \in \mathcal{H}$ and any functions θ and \mathbf{p}^θ , there exists $\phi \in \Phi$ such that

$$\mathbb{E}_{\mu \sim p_\mu} \|\mathbf{p}^\phi(\mathbf{H}, \mu; \phi) - \mathbf{p}^\theta(\mathbf{H}; \theta(\mu))\|_\infty \leq \epsilon. \quad (12)$$

We also introduce an additional assumption on the Lipschitz continuity of the expected utility and performance functions, which we mention below.

Assumption 1. The utility \mathcal{U} and performance function \mathbf{f} are expectation-wise Lipschitz. More precisely, for any pair of ergodic average rate vectors \mathbf{x}_1 and \mathbf{x}_2 , we have

$$\mathbb{E} |\mathcal{U}(\mathbf{x}_1) - \mathcal{U}(\mathbf{x}_2)| \leq \mathbb{E} \|\mathbf{x}_1 - \mathbf{x}_2\|_\infty. \quad (13)$$

Algorithm 1 Training the State-Augmented RRM Algorithm Model Parameters

- 1: **Input:** Number of training iterations N , batch size B , number of time steps T , primal learning rate η_ϕ .
- 2: Initialize: ϕ_0 .
- 3: **for** $n = 0, \dots, N - 1$ **do**
- 4: **for** $b = 0, \dots, B - 1$ **do**
- 5: Randomly sample $\mu_b \sim p_\mu$.
- 6: Randomly generate a sequence of network states $\{H_{b,t}\}_{t=0}^{T-1}$.
- 7: **for** $t = 0, \dots, T - 1$ **do**
- 8: Generate RRM decisions $\mathbf{p}^\phi(\mathbf{H}_{b,t}, \mu_b; \phi_n)$.
- 9: **end for**
- 10: Calculate the augmented Lagrangian according to (9), i.e.,

$$\mathcal{L}_{\mu_b}(\phi_n) = \mathcal{U} \left(\frac{1}{T} \sum_{t=0}^{T-1} \mathbf{f}(\mathbf{H}_{b,t}, \mathbf{p}^\phi(\mathbf{H}_{b,t}, \mu_b; \phi_n)) \right) + \mu^T \mathbf{g} \left(\frac{1}{T} \sum_{t=0}^{T-1} \mathbf{f}(\mathbf{H}_{b,t}, \mathbf{p}^\phi(\mathbf{H}_{b,t}, \mu_b; \phi_n)) \right).$$

- 11: **end for**
- 12: Update the model parameters according to (18), i.e.,

$$\phi_{n+1} = \phi_n + \frac{\eta_\phi}{B} \sum_{b=0}^{B-1} \nabla_\phi \mathcal{L}_{\mu_b}(\phi_n).$$

- 13: **end for**
 - 14: $\phi^* \leftarrow \phi_N$.
 - 15: **Return:** Optimal model parameters ϕ^* .
-

Moreover, given an arbitrary network state \mathbf{H} , there exists a constant M such that any pair of RRM decision functions \mathbf{p}_1 and \mathbf{p}_2 , we have

$$\begin{aligned} \mathbb{E} \|\mathbf{f}(\mathbf{H}, \mathbf{p}_1(\mathbf{H})) - \mathbf{f}(\mathbf{H}, \mathbf{p}_2(\mathbf{H}))\|_\infty \\ \leq M \mathbb{E} \|\mathbf{p}_1(\mathbf{H}) - \mathbf{p}_2(\mathbf{H})\|_\infty. \end{aligned} \quad (14)$$

Note that in (13), we assume that the Lipschitz constant for the utility \mathcal{U} is equal to 1 without loss of generality, as the utility function in the original optimization problem can be scaled by any arbitrary factor without any impact on the solution. Having Definition 1 and Assumption 1, we can now state the following theorem, which shows that the RRM decisions generated by the proposed state-augmented procedure in (10)-(11) are close to the ones made by the original iterative RRM algorithm in (5)-(6).

Theorem 2. *Under the hypotheses of Theorem 1, Assumption 1, and assuming that the state-augmented parameterization $\mathbf{p}^\phi(\mathbf{H}, \mu; \phi)$ is near-universal with degree ϵ in the sense of Definition 1, the RRM decisions made by the state-augmented algorithm in (10)-(11) are both feasible, i.e.,*

$$\lim_{T \rightarrow \infty} \mathbf{g} \left(\frac{1}{T} \sum_{t=0}^{T-1} \mathbf{f}(\mathbf{H}_t, \mathbf{p}^\phi(\mathbf{H}_t, \mu_{\lfloor t/T_0 \rfloor}; \phi^*)) \right) \geq \mathbf{0}, \quad a.s. \quad (15)$$

and near-optimal, i.e.,

$$\begin{aligned} \lim_{T \rightarrow \infty} \mathbb{E} \left[\mathcal{U} \left(\frac{1}{T} \sum_{t=0}^{T-1} \mathbf{f}(\mathbf{H}_t, \mathbf{p}^\phi(\mathbf{H}_t, \mu_{\lfloor t/T_0 \rfloor}; \phi^*)) \right) \right] \\ \geq P^* - \frac{c\eta_\mu G^2}{2} - M\epsilon. \end{aligned} \quad (16)$$

Proof. See Appendix B. □

A. Practical Considerations

In order to resolve the maximization in (10) during the offline training phase, we use a gradient ascent-based approach to learn an optimal set of parameters ϕ^* , which can be frozen after training is complete and utilized during execution. In particular, during the training phase, for a batch of dual variables $\{\mu_b\}_{b=1}^B$, randomly sampled from the distribution p_μ , we consider the *empirical* version of the Lagrangian maximization problem in (10), i.e.,

$$\phi^* = \arg \max_{\phi \in \Phi} \frac{1}{B} \sum_{b=1}^B \mathcal{L}_{\mu_b}(\phi), \quad (17)$$

which we iteratively solve using gradient ascent. More specifically, we randomly initialize the model parameters as ϕ_0 , and then update them over an iteration index $n \in \{0, 1, 2, \dots, N - 1\}$ as

$$\phi_{n+1} = \phi_n + \frac{\eta_\phi}{B} \sum_{b=0}^{B-1} \nabla_\phi \mathcal{L}_{\mu_b}(\phi_n), \quad (18)$$

where η_ϕ denotes the learning rate corresponding to the model parameters ϕ . With a slight abuse of notation, we denote the final set of model parameters (i.e., the outcome of (18) upon convergence) as ϕ^* . Note that to enhance the generalization capability of the trained model, for each set of dual variables $\mu_b, b \in \{0, 1, 2, \dots, B\}$, in the batch, we can also randomly sample a separate realization of the sequence of network states, i.e., $\{H_{b,t}\}_{t=0}^{T-1}$, from the underlying random process, allowing the model to be optimized over a *family* of network realizations. The training procedure is summarized in Algorithm 1.

During execution, the dual dynamics are used to update the

Algorithm 2 Execution Phase for the State-Augmented RRM Algorithm

- 1: **Input:** Optimal model parameters ϕ^* , sequence of network states $\{H_t\}_{t=0}^{T-1}$, iteration length T_0 , dual learning rate η_μ .
- 2: Initialize: $\mu_0 \leftarrow \mathbf{0}, k \leftarrow 0$.
- 3: **for** $t = 0, \dots, T - 1$ **do**
- 4: Generate RRM decisions $\mathbf{p}_t := \mathbf{p}^\phi(\mathbf{H}_t, \mu_k; \phi^*)$.
- 5: **if** $t + 1 \bmod T_0 = 0$ **then**
- 6: Update the dual variables according to (11), i.e.,

$$\mu_{k+1} = \left[\mu_k - \eta_\mu \mathbf{g} \left(\frac{1}{T_0} \sum_{t=kT_0}^{(k+1)T_0-1} \mathbf{f}(\mathbf{H}_t, \mathbf{p}^\phi(\mathbf{H}_t, \mu_k; \phi^*)) \right) \right]_+.$$

- 7: $k \leftarrow k + 1$.
 - 8: **end if**
 - 9: **end for**
 - 10: **Return:** Sequence of RRM decisions $\{\mathbf{p}_t\}_{t=0}^{T-1}$.
-

dual variables and generate the RRM decisions as follows: We initialize the dual variables as $\mu_0 = \mathbf{0}$. For any time step $t \in \{0, 1, 2, \dots, T - 1\}$, given the network state \mathbf{H}_t , we generate the RRM decisions using the state-augmented RRM policy $\mathbf{p}(\mathbf{H}_t, \mu_{\lfloor t/T_0 \rfloor}; \phi^*)$. Then, we update the dual variables every T_0 time steps as in (11). Note how the dual dynamics in (11) track the satisfaction of the original constraints in (2b). In particular, if the RRM decisions at time step t help satisfy the constraints, the dual variables are reduced. On the other hand, if the constraints are not satisfied at a given time step, the dual variables increase in value. The state-augmented execution procedure is summarized in Algorithm 2.

Remark 1. Note that the choice of distribution p_μ for sampling the dual variables during training can affect the optimal model parameters ϕ^* . As we will show in Section V-B, a uniform distribution provides a desirable performance in our experiments. However, according to the dual dynamics in (11), sampling the dual variables from the dual descent trajectory might lead to superior performance. Such a distribution may also be dependent on the realization of the initial network state, \mathbf{H}_0 . The problem of finding the best distribution for sampling dual variables during training is an interesting research direction, which we leave as future work.

Remark 2. The RRM decisions $\mathbf{p}^\phi(\mathbf{H}_t, \mu_{\lfloor t/T_0 \rfloor}; \phi^*)$ generated by our proposed algorithm might be suboptimal before the convergence of the dual variables. This implies that it might be beneficial to either i) have a number of warm-up time steps at the beginning of the execution phase until optimal RRM decisions are generated, or ii) initialize the dual variables with their optimal levels, which can be possible for network realizations seen during training, but does not necessarily transfer across different network realizations.

V. APPLICATION TO POWER CONTROL WITH GRAPH NEURAL NETWORK PARAMETERIZATIONS

As an important application of the RRM problem to showcase the capabilities of the proposed state-augmented learning algorithm, we consider the problem of power control

in m -user interference channels. More precisely, we study networks comprising m users, i.e., transmitter-receiver pairs $\{(T_x, R_x)\}_{x=1}^m$, where each transmitter intends to communicate to its corresponding receiver, while causing interference at other receivers. In this setting, the network state at time step t , i.e., $\mathbf{H}_t \in \mathbb{C}^{m \times m}$, contains all channel gains in the network, where the channel gain between transmitter T_x and receiver R_x at time step t is denoted by $h_{x,t} \in \mathbb{C}$. The RRM decisions $\mathbf{p} \in [0, P_{\max}]^m$ represent the transmit power levels of the transmitters, with P_{\max} denoting the maximum transmit power. Moreover, the performance function $\mathbf{f}(\mathbf{H}_t, \mathbf{p}) \in \mathbb{R}^m$ represents the receiver rates, where for each receiver R_x , the rate at time step t is given by

$$f_i(\mathbf{H}_t, \mathbf{p}) = \log_2 \left(1 + \frac{p_i |h_{ii,t}|^2}{N + \sum_{j=1, j \neq i}^m p_j |h_{ji,t}|^2} \right), \quad (19)$$

where N denotes the noise variance, and it is assumed that the receiver treats all incoming interference as noise [28], [29].

We use a sum-rate utility $\mathcal{U}(\mathbf{x}) = \sum_{i=1}^m x_i$, and consider per-user minimum-rate requirements as the constraints. In particular, we consider $c = m$ constraints, where the i^{th} constraint is given by $g_i(\mathbf{x}) = x_i - f_{\min}$, with f_{\min} denoting the minimum per-user rate requirement.

A. GNN-Based Parameterizations

In order to parameterize the state-augmented RRM policy, as in prior work [9], [17], [19], [30], we use graph neural network (GNN) architectures, which have been shown to provide several benefits, such as scalability, transferability, and permutation-equivariance. We operate the GNN over a graph-structured format of the interference channel, defined as a graph $\mathcal{G}_t = (\mathcal{V}, \mathcal{E}, \mathbf{y}_t, w_t)$ at each time step t , where:

- $\mathcal{V} = \{1, 2, \dots, m\}$ denotes the set of graph nodes, with each node representing a user (i.e., transmitter-receiver pair) in the graph,
- $\mathcal{E} = \mathcal{V} \times \mathcal{V}$ denotes the set of directed graph edges,
- $\mathbf{Y}_t \in \mathbb{R}^{m \times 1}$ denotes the initial node features, which we set to the dual variables associated to the users at each time step, i.e., $\mathbf{Y}_t := \mu_{\lfloor t/T_0 \rfloor}$, and

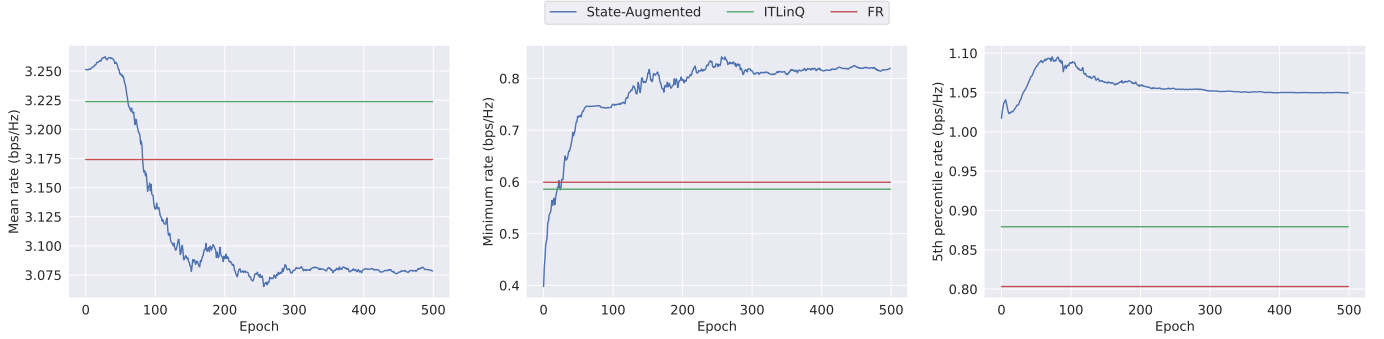


Fig. 1: Convergence behavior of the proposed state-augmented RRM algorithm, and its comparison with the baseline methods for a single network realization with $m = 40$ transmitter-receiver pairs (fixed-density scenario). Note that the baseline algorithms fail to achieve the minimum-rate requirement of $f_{\min} = 3/4$, while our proposed method is able to satisfy the constraints for all users.

- $w_t : \mathcal{E} \rightarrow \mathbb{R}$ denotes the function that maps each edge to its weight at time t , which we define as $w_t(i, j) := \frac{1}{Z_t} \log(P_{\max}|h_{ij,t}|^2/N)$, with $Z_t > 0$ representing a normalization factor.

Note how the aforementioned graph structure allows the implementation of the state-augmented architecture, where the GNN can take the dual variables corresponding to all the users as the input node features, and the network state as the input edge features. More precisely, we consider L consecutive GNN message-passing layers, where the l^{th} layer, $l \in \{1, 2, \dots, L\}$ transforms the node features at layer $l-1$, i.e., $\mathbf{Y}_t^{l-1} \in \mathbb{R}^{m \times F_{l-1}}$, to the node features at layer l , i.e., $\mathbf{Y}_t^l \in \mathbb{R}^{m \times F_l}$. In its most general form, for each node $v \in \mathcal{V}$, the aforementioned update can be written as

$$\mathbf{y}_{v,t}^l = \Psi^l \left(\{ \mathbf{y}_{u,t}^{l-1}, w_t(u, v) \}_{u \in \mathcal{V}: (u,v) \in \mathcal{E}}; \phi^l \right), \quad (20)$$

where $\Psi^l(\cdot; \phi^l) : \mathbb{R}^{F_{l-1}} \rightarrow \mathbb{R}^{F_l}$ denotes the message-passing GNN operator, parameterized by the set of parameters ϕ^l . We use $\mathbf{Y}_t^0 = \mathbf{Y}_t$ (with $F_0 = 1$) as the initial node features. We also set $F_L = 1$ to produce a scalar output feature per node, and we define the power control decisions as

$$\mathbf{p}^\phi \left(\mathbf{H}_t, \boldsymbol{\mu}_{\lfloor t/T_0 \rfloor}; \phi \right) := P_{\max} \cdot \sigma(\mathbf{Y}_t^L), \quad (21)$$

where $\phi := \{ \phi^l \}_{l=1}^L$, and $\sigma(\cdot)$ denotes element-wise sigmoid function, with $\sigma(x) = \frac{1}{1 + \exp(-x)}$, $\forall x \in \mathbb{R}$, which is used to respect the instantaneous power level constraints $\mathbf{p} \in [0, P_{\max}]^m$.

B. Experimental Results

We generate networks with m transmitter-receiver pairs, located randomly within a square network area of side length R . We drop the transmitters uniformly at random within the network area, while ensuring a minimum distance of 35m between each pair of them. Afterwards, for each transmitter, we drop its associated receiver uniformly at random within an annulus around the transmitter, with inner and outer radii of 10m and 50m, respectively. To control the network density, we consider the following two scenarios to determine the network area size:

- **Fixed Density:** We set $R = \sqrt{m/20} \times 1\text{km}$ to keep the density constant at 20 users/km².
- **Variable Density:** We set $R = 500\text{m}$, implying that the network density increases with m .

In both cases, and for all values of m , we set $f_{\min} = \frac{3}{4}$ bps/Hz, $T_0 = 5$, and $T = 100$. We consider both large-scale and small-scale fading for the channel model. The large-scale fading follows a dual-slope path-loss model similar to [17], [31], [32] alongside a 7dB log-normal shadowing. Moreover, the small-scale fading models channel variations across different time steps following a Rayleigh distribution with a pedestrian speed of 1m/s [33]. We set the maximum transmit power to $P_{\max} = 10\text{dBm}$, and the noise variance to $N = -104\text{dBm}$ (due to the 10MHz bandwidth and noise power spectral density of -174dBm/Hz).

We use a 3-layer GNN with $F_1 = F_2 = 64$, where the first two layers are based on the local extremum operator proposed in [34], while the last layer entails a linear projection (together with the mapping in (21)). We set the primal and dual learning rates to $\eta_\phi = 10^{-1}/m$ and $\eta_\mu = 2$, respectively, and we set the batch size to $B = 128$. For each value of m , we generate a total of 256 training samples and 128 samples for evaluation, where each sample refers to a realization of the transmitter/receiver locations (and the large-scale fading), alongside the small-scale fading random process. We set the normalization factor for edge weights at time step t to $Z_t = \|\log(P_{\max}|\mathbf{H}_t|^2/N)\|_2$. Except for the case of Section V-B1 below, we run training for 100 epochs, and we draw the dual variables during training randomly from the $U(0, 1)$ distribution.

As baselines, we compare the performance of our proposed method against full reuse (FR), where every transmitter uses P_{\max} , and ITLinQ [3]. We mainly report the results in terms of three separate metrics, namely the mean rate, minimum rate, and the 5th percentile rate, evaluated over the test configurations.¹

1) *Single Network Realization:* Figure 1 shows the performance of our proposed method against the baselines for a single network realization with $m = 40$ users (in the fixed-density scenario). For this specific experiment, we continue

¹Our code is available at https://github.com/navid-naderi/StateAugmented_RRM_GNN.

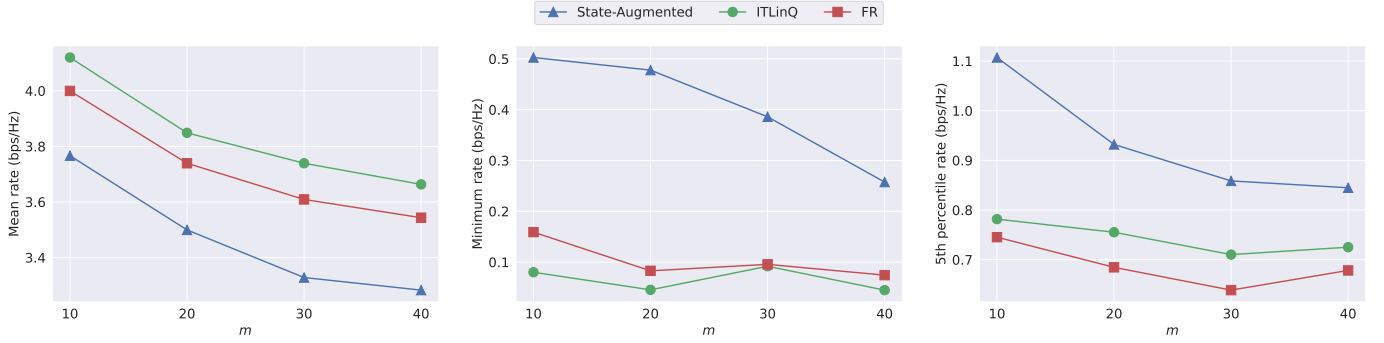


Fig. 2: Performance comparison of the proposed state-augmented RRM algorithm against baseline methods in the fixed-density scenario for networks with $m \in \{10, 20, 30, 40\}$ transmitter-receiver pairs.

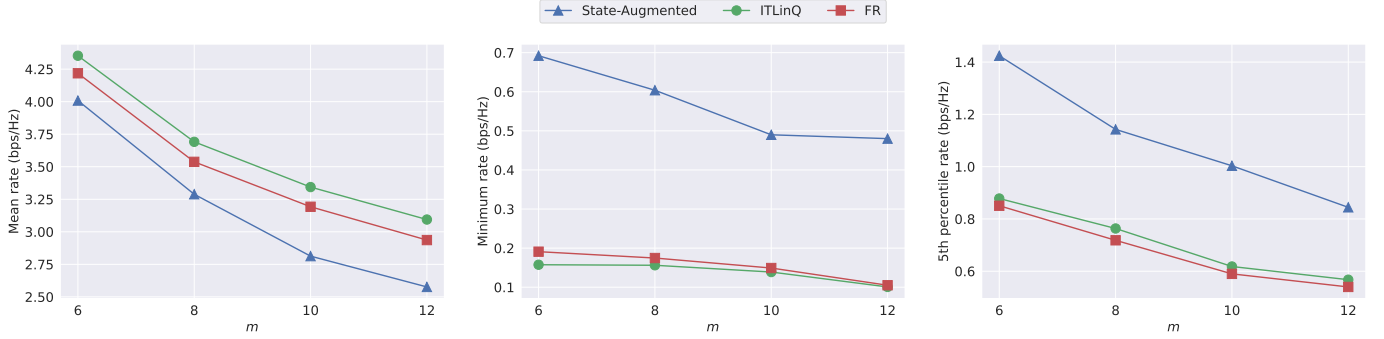


Fig. 3: Performance comparison of the proposed state-augmented RRM algorithm against baseline methods in the variable-density scenario for networks with $m \in \{6, 8, 10, 12\}$ transmitter-receiver pairs.

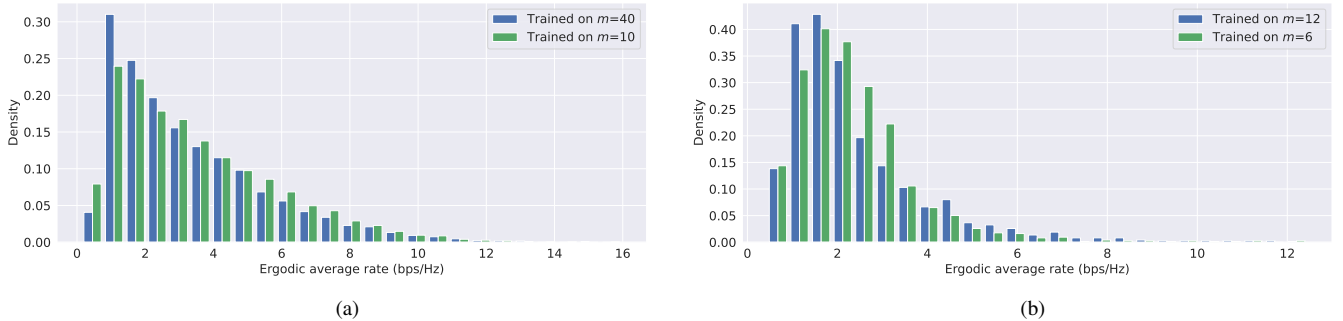


Fig. 4: Transferability of the proposed state-augmented RRM procedure, shown as the histogram of ergodic average rates, for the (a) fixed-density scenario, evaluated on samples with $m = 40$, and (b) variable-density scenario, evaluated on samples with $m = 12$.

training for 500 epochs, and decay the primal learning rate by 0.5 every 100 epochs. At the end of each training epoch, we evaluate the RRM algorithm on the same realization that is used for training. As the figure shows, our proposed state-augmented RRM algorithm considerably gains over the baseline algorithms in terms of the minimum and 5th percentile rates, managing to satisfy the minimum-rate requirements for all users at the expense of a smaller achieved mean rate.

2) *Scalability*: Here, we assess the performance of the GNN-based RRM policies in families of networks with different numbers of users, where the policies trained on samples with a specific value of m are evaluated on test samples with the same value of m . Figures 2 and 3 compare the performance of our proposed method with the baseline algorithms in the fixed-density and variable-density scenarios, respectively. In

both scenarios, thanks to the per-user minimum-rate constraints, our method significantly outperforms the baseline methods in terms of the minimum rate and the 5th percentile rate. This, however, comes at the cost of a slightly lower mean rate compared to ITLinQ and full reuse. Note that such a scalability is due to the size-invariant property of GNN-based parameterizations (where the number of parameters is fixed regardless of the graph size), as opposed to other parameterization, such as multi-layer perceptrons (i.e., fully-connected neural networks).

3) *Transferability to Unseen Network Sizes*: Another upside of the size-invariance property of GNNs is that they can be evaluated on graph sizes not encountered throughout the training process. Figure 4a shows the histogram of user ergodic average rates in test networks of size $m = 40$ (fixed-density

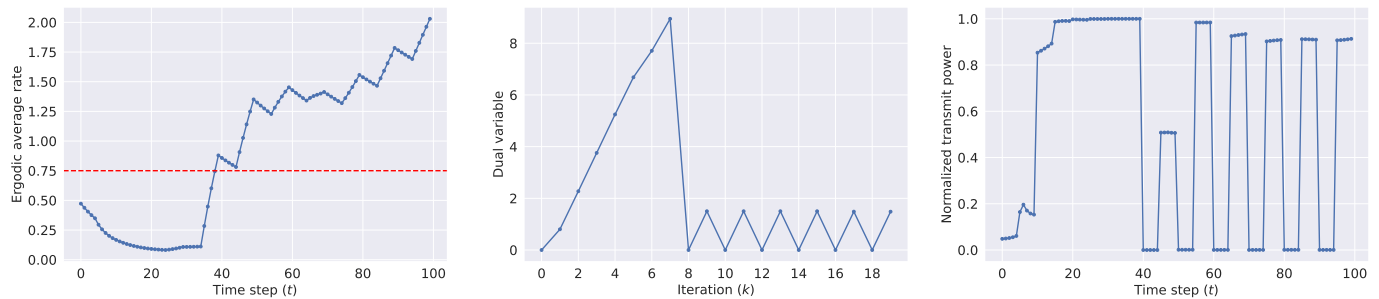


Fig. 5: Evolution of the ergodic average rate (left), dual variable (middle), and normalized transmit power level (right) for an example user in a network with $m = 6$ transmitter-receiver pairs (for the variable-density scenario). The dashed red line in the left plot shows the minimum-rate requirement, i.e., $f_{\min} = \frac{3}{4}$.

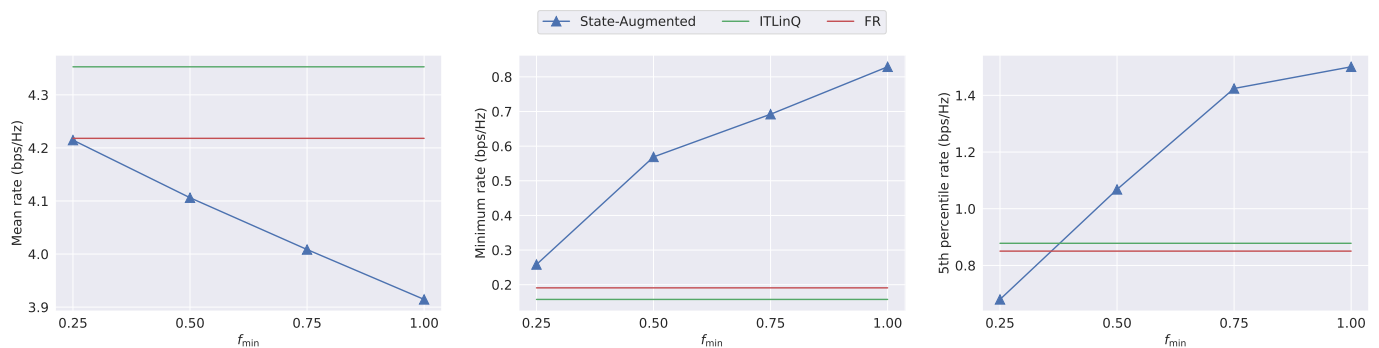


Fig. 6: Impact of the minimum-rate constraint lower bound, f_{\min} , on the performance achieved by the proposed state-augmented RRM algorithm in networks with $m = 6$ transmitter-receiver pairs (for the variable-density scenario).

scenario) using two GNNs: one trained on samples with $m = 40$ and the other trained on samples with $m = 10$. Moreover, Figure 4b shows a similar histogram for the variable-density scenario, where GNNs trained on samples with $m = 12$ and $m = 6$ are evaluated on test samples with $m = 12$. As the figures show, in both cases, the trained GNNs provide excellent transferability to larger network sizes, achieving user rates that are similar to the GNNs without the train/test mismatch. Moreover, as expected, the transferred performance is more desirable in the fixed-density scenario than the variable-density scenario, as the channel statistics mostly remain similar in the former case, while in the latter case, the network becomes more interference-limited as m grows.

4) *Policy Switching*: Figure 5 shows what an example receiver experiences over the course of the $T = 100$ time steps in a test network with $m = 6$ transmitter-receiver pairs (for the variable-density scenario) once training is completed. Letting i denote the receiver index, at each time step t , we plot its ergodic average rate up to that time step (i.e., $\frac{1}{t} \sum_{\tau=1}^t f_i(\mathbf{H}_{\tau}, \mathbf{p}^{\phi}(\mathbf{H}_{\tau}, \boldsymbol{\mu}_{\lfloor \tau/T_0 \rfloor}; \boldsymbol{\phi}^*))$), its dual variable at the corresponding iteration (i.e., $\mu_{i, \lfloor t/T_0 \rfloor}$), and the selected normalized transmit power of transmitter i at that time step (i.e., $p_i^{\phi}(\mathbf{H}_t, \boldsymbol{\mu}_{\lfloor t/T_0 \rfloor}; \boldsymbol{\phi}^*)/P_{\max}$). As the figure shows, a *policy switching* behavior occurs, where for the time steps in which the receiver's ergodic average rate is below f_{\min} , the dual variable increases, leading to the corresponding transmitter using full transmit power. Moreover, when the ergodic average rate exceeds f_{\min} , the transmitter uses an on-off pattern to maintain its receiver's high ergodic average rate,

while minimizing the interference caused at other receivers. This shows why state-augmentation is crucial for the algorithm to be able to switch the policy if/when necessary, depending on the constraint violations over time.

5) *Impact of the Minimum-Rate Constraint Lower Bounds*: In all our experiments, we set the lower bounds for the minimum-rate constraints, i.e., f_{\min} to $\frac{3}{4}$. This resulted in RRM decisions that attempted to satisfy relatively strict minimum-rate constraints for almost all network realizations, which came at the cost of lower mean rates as compared to baseline methods. Figure 6 demonstrates the impact of the constraint lower bounds $f_{\min} \in \{\frac{1}{4}, \frac{1}{2}, \frac{3}{4}, 1\}$ on the performance of the proposed state-augmented RRM algorithm when trained and evaluated on networks with $m = 6$ transmitter-receiver pairs (in the variable-density scenario). As the figure shows, tuning f_{\min} reveals the trade-off between the average and worst-case performance of users across all network realizations. Finding the best minimum-rate constraint lower bound is a non-trivial problem, and it has also been shown that this bound can be tuned adaptively based on each specific network realization through the introduction of learnable slack parameters [17], [35], [36]. We leave the incorporation of adaptive minimum-rate constraints into state-augmented RRM algorithms as future work.

VI. CONCLUDING REMARKS

We considered the problem of resource allocation in wireless network, termed radio resource management (RRM), in which the goal is to maximize a network-wide utility

subject to constraints on the long-term average performance of the network users. We showed how parameterized dual-based RRM policies can lead to feasible and near-optimal solutions, but suffer from multiple challenges, including that they need to be run for an infinite number of time steps and the model parameters have to be optimized for any given set of dual variables at every time step. To mitigate these challenges, we proposed a state-augmented RRM algorithm, which revises the parameterization to take as input the network state, as well as the dual variable at each step, and produce as output the RRM decisions. We showed that for near-universal parameterizations, the proposed method also leads to feasible and near-optimal sequences of RRM decisions. Using graph neural network (GNN) architectures to parameterize the state-augmented RRM policy, we also demonstrated, via a set of numerical experiments, that the proposed method provides scalable and transferable wireless power control solutions that outperform baseline algorithms.

REFERENCES

- [1] Q. Shi, M. Razaviyayn, Z.-Q. Luo, and C. He, "An iteratively weighted MMSE approach to distributed sum-utility maximization for a MIMO interfering broadcast channel," *IEEE Transactions on Signal Processing*, vol. 59, no. 9, pp. 4331–4340, 2011.
- [2] X. Wu, S. Tavildar, S. Shakkottai, T. Richardson, J. Li, R. Laroya, and A. Jovicic, "FlashLinQ: A synchronous distributed scheduler for peer-to-peer ad hoc networks," *IEEE/ACM Transactions on Networking*, vol. 21, no. 4, pp. 1215–1228, 2013.
- [3] N. Naderializadeh and A. S. Avestimehr, "ITLinQ: A new approach for spectrum sharing in device-to-device communication systems," *IEEE Journal on Selected Areas in Communications*, vol. 32, no. 6, pp. 1139–1151, 2014.
- [4] X. Yu and G. Caire, "ITLinQ+: An improved spectrum sharing mechanism for device-to-device communications," in *2015 49th Asilomar Conference on Signals, Systems and Computers*. IEEE, 2015, pp. 1310–1314.
- [5] K. Shen and W. Yu, "FPLinQ: A cooperative spectrum sharing strategy for device-to-device communications," in *2017 IEEE International Symposium on Information Theory (ISIT)*. IEEE, 2017, pp. 2323–2327.
- [6] M. Eisen, C. Zhang, L. F. Chamon, D. D. Lee, and A. Ribeiro, "Learning optimal resource allocations in wireless systems," *IEEE Transactions on Signal Processing*, vol. 67, no. 10, pp. 2775–2790, 2019.
- [7] Y. S. Nasir and D. Guo, "Multi-agent deep reinforcement learning for dynamic power allocation in wireless networks," *IEEE Journal on Selected Areas in Communications*, vol. 37, no. 10, pp. 2239–2250, 2019.
- [8] L. Liang, H. Ye, G. Yu, and G. Y. Li, "Deep-learning-based wireless resource allocation with application to vehicular networks," *Proceedings of the IEEE*, 2019.
- [9] M. Eisen and A. Ribeiro, "Optimal wireless resource allocation with random edge graph neural networks," *IEEE Transactions on Signal Processing*, vol. 68, pp. 2977–2991, 2020.
- [10] Y. Shen, Y. Shi, J. Zhang, and K. B. Letaief, "Graph neural networks for scalable radio resource management: Architecture design and theoretical analysis," *IEEE Journal on Selected Areas in Communications*, vol. 39, no. 1, pp. 101–115, 2020.
- [11] N. Naderializadeh, J. J. Sydir, M. Simsek, and H. Nikopour, "Resource management in wireless networks via multi-agent deep reinforcement learning," *IEEE Transactions on Wireless Communications*, vol. 20, no. 6, pp. 3507–3523, 2021.
- [12] S. Niknam, A. Roy, H. S. Dhillon, S. Singh, R. Banerji, J. H. Reed, N. Saxena, and S. Yoon, "Intelligent o-ran for beyond 5g and 6g wireless networks," *arXiv preprint arXiv:2005.08374*, 2020.
- [13] L. Bonati, S. D'Oro, M. Polese, S. Basagni, and T. Melodia, "Intelligence and learning in o-ran for data-driven nextg cellular networks," *IEEE Communications Magazine*, vol. 59, no. 10, pp. 21–27, 2021.
- [14] K. B. Letaief, Y. Shi, J. Lu, and J. Lu, "Edge artificial intelligence for 6g: Vision, enabling technologies, and applications," *IEEE Journal on Selected Areas in Communications*, vol. 40, no. 1, pp. 5–36, 2021.
- [15] "6G vision white paper: Mediatek's vision for the next-generation of cellular mobile technologies," MediaTek, Tech. Rep., January 2022. [Online]. Available: <https://www.mediatek.com/blog/6g-whitepaper>
- [16] A. Ribeiro, "Optimal resource allocation in wireless communication and networking," *EURASIP Journal on Wireless Communications and Networking*, vol. 2012, no. 1, pp. 1–19, 2012.
- [17] N. Naderializadeh, M. Eisen, and A. Ribeiro, "Learning resilient radio resource management policies with graph neural networks," *arXiv preprint arXiv:2203.11012*, 2022.
- [18] M. Calvo-Fullana, S. Paternain, L. F. Chamon, and A. Ribeiro, "State augmented constrained reinforcement learning: Overcoming the limitations of learning with rewards," *arXiv preprint arXiv:2102.11941*, 2021.
- [19] M. Lee, G. Yu, and G. Y. Li, "Graph embedding-based wireless link scheduling with few training samples," *IEEE Transactions on Wireless Communications*, vol. 20, no. 4, pp. 2282–2294, 2020.
- [20] Z. Wang, M. Eisen, and A. Ribeiro, "Learning decentralized wireless resource allocations with graph neural networks," *arXiv e-prints*, pp. arXiv–2107, 2021.
- [21] N. Naderializadeh, "Wireless link scheduling via graph representation learning: A comparative study of different supervision levels," *arXiv preprint arXiv:2110.01722*, 2021.
- [22] A. Chowdhury, G. Verma, C. Rao, A. Swami, and S. Segarra, "Unfolding wmmse using graph neural networks for efficient power allocation," *IEEE Transactions on Wireless Communications*, vol. 20, no. 9, pp. 6004–6017, 2021.
- [23] Z. Wang, M. Eisen, and A. Ribeiro, "Unsupervised learning for asynchronous resource allocation in ad-hoc wireless networks," in *ICASSP 2021-2021 IEEE International Conference on Acoustics, Speech and Signal Processing (ICASSP)*. IEEE, 2021, pp. 8143–8147.
- [24] Z. Zhao, G. Verma, C. Rao, A. Swami, and S. Segarra, "Link scheduling using graph neural networks," *arXiv preprint arXiv:2109.05536*, 2021.
- [25] I. Nikoloska and O. Simeone, "Modular meta-learning for power control via random edge graph neural networks," *arXiv preprint arXiv:2108.13178*, 2021.
- [26] A. Chowdhury, G. Verma, C. Rao, A. Swami, and S. Segarra, "Efficient power allocation using graph neural networks and deep algorithm unfolding," in *ICASSP 2021-2021 IEEE International Conference on Acoustics, Speech and Signal Processing (ICASSP)*. IEEE, 2021, pp. 4725–4729.
- [27] B. Li, A. Swami, and S. Segarra, "Power allocation for wireless federated learning using graph neural networks," in *ICASSP 2022-2022 IEEE International Conference on Acoustics, Speech and Signal Processing (ICASSP)*. IEEE, 2022, pp. 5243–5247.
- [28] V. S. Annapureddy and V. V. Veeravalli, "Gaussian interference networks: Sum capacity in the low-interference regime and new outer bounds on the capacity region," *IEEE Transactions on Information Theory*, vol. 55, no. 7, pp. 3032–3050, 2009.
- [29] C. Geng, N. Naderializadeh, A. S. Avestimehr, and S. A. Jafar, "On the optimality of treating interference as noise," *IEEE Transactions on Information Theory*, vol. 61, no. 4, pp. 1753–1767, 2015.
- [30] Y. Shen, Y. Shi, J. Zhang, and K. B. Letaief, "A graph neural network approach for scalable wireless power control," *arXiv preprint arXiv:1907.08487*, 2019.
- [31] X. Zhang and J. G. Andrews, "Downlink cellular network analysis with multi-slope path loss models," *IEEE Transactions on Communications*, vol. 63, no. 5, pp. 1881–1894, 2015.
- [32] J. G. Andrews, X. Zhang, G. D. Durgin, and A. K. Gupta, "Are we approaching the fundamental limits of wireless network densification?" *IEEE Communications Magazine*, vol. 54, no. 10, pp. 184–190, 2016.
- [33] Y. Li and X. Huang, "The simulation of independent Rayleigh faders," *IEEE Transactions on Communications*, vol. 50, no. 9, pp. 1503–1514, 2002.
- [34] E. Ranjan, S. Sanyal, and P. Talukdar, "ASAP: Adaptive structure aware pooling for learning hierarchical graph representations," *Proceedings of the AAAI Conference on Artificial Intelligence*, vol. 34, no. 04, pp. 5470–5477, 2020.
- [35] N. Naderializadeh, M. Eisen, and A. Ribeiro, "Wireless power control via counterfactual optimization of graph neural networks," in *2020 IEEE 21st International Workshop on Signal Processing Advances in Wireless Communications (SPAWC)*. IEEE, 2020, pp. 1–5.
- [36] N. Naderializadeh, M. Eisen, and A. Ribeiro, "Adaptive wireless power allocation with graph neural networks," in *ICASSP 2022-2022 IEEE International Conference on Acoustics, Speech and Signal Processing (ICASSP)*. IEEE, 2022, pp. 5213–5217.
- [37] A. Ribeiro, "Ergodic stochastic optimization algorithms for wireless communication and networking," *IEEE Transactions on Signal Processing*, vol. 58, no. 12, pp. 6369–6386, 2010.

- [38] J. M. Danskin, *The theory of max-min and its application to weapons allocation problems*. Springer Science & Business Media, 2012, vol. 5.
 [39] S. Boyd, S. P. Boyd, and L. Vandenberghe, *Convex optimization*. Cambridge university press, 2004.

APPENDIX A
 PROOF OF THEOREM 1

The arguments used in the proof of Theorem 1 follow similar steps to those in [18], [37]. However, there are differences with prior proofs, specific to our problem formulation, that require us to include the complete proof here.

A. Tightness of The Sequence of Dual Variable Probability Measures

We start by proving that the sequence of dual variable probability measures, i.e., $\{p(\boldsymbol{\mu}_k | \boldsymbol{\mu}_0)\}_k$, is tight in the following lemma.

Lemma 1. *For any $\delta > 0$, there exists a compact set \mathcal{A}_δ such that for every $k \geq 0$, we have $\Pr[\boldsymbol{\mu}_k \in \mathcal{A}_\delta] > 1 - \delta$.*

Proof. Define the dual function, $d(\boldsymbol{\mu})$ as

$$d(\boldsymbol{\mu}) = \max_{\boldsymbol{\theta} \in \Theta} \mathcal{L}(\boldsymbol{\theta}, \boldsymbol{\mu}), \quad (22)$$

and consider the following set:

$$\mathcal{C} = \left\{ \boldsymbol{\mu} \in \mathbb{R}_+^c : d(\boldsymbol{\mu}) - P^* \leq \frac{c\eta_\mu G^2}{2} \right\}. \quad (23)$$

Now, let

$$\mathcal{A}_\delta = \mathcal{B}_\delta \cup \left(\mathcal{C} \oplus \mathcal{S}_{\sqrt{c\eta_\mu^2 G^2}} \right), \quad (24)$$

where \oplus denotes Minkowski sum, \mathcal{S}_r denotes a ball centered at the origin with radius $r \geq 0$, and \mathcal{B}_δ is defined as

$$\mathcal{B}_\delta = \left\{ \boldsymbol{\mu} \in \mathbb{R}_+^c : \frac{\|\boldsymbol{\mu} - \boldsymbol{\mu}^*\|}{\|\boldsymbol{\mu}_0 - \boldsymbol{\mu}^*\|} \leq \frac{1}{\delta} \right\}, \quad (25)$$

with $\boldsymbol{\mu}^*$ representing the optimal set of dual variables. Then, we have

$$\begin{aligned} & \Pr[\boldsymbol{\mu}_k \in \mathcal{A}_\delta] \\ &= \Pr \left[\boldsymbol{\mu}_k \in \mathcal{B}_\delta \cup \left(\mathcal{C} \oplus \mathcal{S}_{\sqrt{c\eta_\mu^2 G^2}} \right) \right] \\ &= \Pr \left[\underbrace{\boldsymbol{\mu}_k \in \mathcal{B}_\delta \cup \left(\mathcal{C} \oplus \mathcal{S}_{\sqrt{c\eta_\mu^2 G^2}} \right)}_{\stackrel{(a)}{=} 1} \mid \boldsymbol{\mu}_{k-1} \in \mathcal{C} \right] \cdot p \\ & \quad + \Pr \left[\underbrace{\boldsymbol{\mu}_k \in \mathcal{B}_\delta \cup \left(\mathcal{C} \oplus \mathcal{S}_{\sqrt{c\eta_\mu^2 G^2}} \right)}_{\geq \Pr[\boldsymbol{\mu}_k \in \mathcal{B}_\delta \mid \boldsymbol{\mu}_{k-1} \in \mathcal{C}^c]} \mid \boldsymbol{\mu}_{k-1} \in \mathcal{C}^c \right] \cdot (1-p) \\ & \geq \Pr \left[\boldsymbol{\mu}_k \in \mathcal{B}_\delta \mid \boldsymbol{\mu}_{k-1} \in \mathcal{C} \right] \\ &= \Pr \left[\frac{\|\boldsymbol{\mu}_k - \boldsymbol{\mu}^*\|}{\|\boldsymbol{\mu}_0 - \boldsymbol{\mu}^*\|} \leq \frac{1}{\delta} \mid \boldsymbol{\mu}_{k-1} \in \mathcal{C} \right] \\ & \geq 1 - \left(\frac{\mathbb{E} [\|\boldsymbol{\mu}_k - \boldsymbol{\mu}^*\| \mid \boldsymbol{\mu}_{k-1} \in \mathcal{C}^c]}{\|\boldsymbol{\mu}_0 - \boldsymbol{\mu}^*\|} \right) \delta, \end{aligned} \quad (26)$$

$$\geq \Pr \left[\frac{\|\boldsymbol{\mu}_k - \boldsymbol{\mu}^*\|}{\|\boldsymbol{\mu}_0 - \boldsymbol{\mu}^*\|} \leq \frac{1}{\delta} \mid \boldsymbol{\mu}_{k-1} \in \mathcal{C}^c \right] \quad (27)$$

$$\geq 1 - \left(\frac{\mathbb{E} [\|\boldsymbol{\mu}_k - \boldsymbol{\mu}^*\| \mid \boldsymbol{\mu}_{k-1} \in \mathcal{C}^c]}{\|\boldsymbol{\mu}_0 - \boldsymbol{\mu}^*\|} \right) \delta, \quad (28)$$

where $p = \Pr[\boldsymbol{\mu}_{k-1} \in \mathcal{C}]$, (a) is true due to the dual dynamics in (6) and the fact that the change between $\boldsymbol{\mu}_{k-1}$ and $\boldsymbol{\mu}_k$ is upper bounded in norm by $\sqrt{c\eta_\mu^2 G^2}$, and the last inequality is

due to conditional Markov's inequality. Therefore, to complete the proof, it suffices to show that (i)

$$\mathbb{E} [\|\boldsymbol{\mu}_k - \boldsymbol{\mu}^*\| \mid \boldsymbol{\mu}_{k-1} \in \mathcal{C}^c] < \|\boldsymbol{\mu}_0 - \boldsymbol{\mu}^*\|, \quad (30)$$

and (ii) that \mathcal{A}_δ is compact.

Proof of (30). Let $\Delta_{\boldsymbol{\mu}_{k-1}}$ be defined as

$$\Delta_{\boldsymbol{\mu}_{k-1}} := \mathbf{g} \left(\frac{1}{T_0} \sum_{t=(k-1)T_0}^{kT_0-1} \mathbf{f}(\mathbf{H}_t, \mathbf{p}^\theta(\mathbf{H}_t; \boldsymbol{\theta}_{k-1})) \right). \quad (31)$$

Then, from the dual dynamics in (6), we have

$$\begin{aligned} & \|\boldsymbol{\mu}_k - \boldsymbol{\mu}^*\|^2 \\ & \leq \|\boldsymbol{\mu}_{k-1} - \boldsymbol{\mu}^* - \eta_\mu \Delta_{\boldsymbol{\mu}_{k-1}}\|^2 \\ & = \|\boldsymbol{\mu}_{k-1} - \boldsymbol{\mu}^*\|^2 + \eta_\mu^2 \|\Delta_{\boldsymbol{\mu}_{k-1}}\|^2 \\ & \quad - 2\eta_\mu (\boldsymbol{\mu}_{k-1} - \boldsymbol{\mu}^*)^T \Delta_{\boldsymbol{\mu}_{k-1}} \\ & \leq \|\boldsymbol{\mu}_{k-1} - \boldsymbol{\mu}^*\|^2 + c\eta_\mu^2 G^2 - 2\eta_\mu (\boldsymbol{\mu}_{k-1} - \boldsymbol{\mu}^*)^T \Delta_{\boldsymbol{\mu}_{k-1}}, \end{aligned}$$

where the last inequality follows from the fact that for any $i \in \{1, \dots, c\}$, we assume $|g_i(\cdot)| \leq G$. Taking the expectation of both sides conditioned on $\boldsymbol{\mu}_{k-1}$, we have

$$\begin{aligned} & \mathbb{E} [\|\boldsymbol{\mu}_k - \boldsymbol{\mu}^*\|^2 \mid \boldsymbol{\mu}_{k-1}] \\ & \leq \|\boldsymbol{\mu}_{k-1} - \boldsymbol{\mu}^*\|^2 + c\eta_\mu^2 G^2 \\ & \quad - 2\eta_\mu (\boldsymbol{\mu}_{k-1} - \boldsymbol{\mu}^*)^T \mathbb{E} [\Delta_{\boldsymbol{\mu}_{k-1}} \mid \boldsymbol{\mu}_{k-1}] \end{aligned} \quad (32)$$

$$\leq \|\boldsymbol{\mu}_{k-1} - \boldsymbol{\mu}^*\|^2 + c\eta_\mu^2 G^2 - 2\eta_\mu (d(\boldsymbol{\mu}_{k-1}) - d(\boldsymbol{\mu}^*)) \quad (33)$$

$$= \|\boldsymbol{\mu}_{k-1} - \boldsymbol{\mu}^*\|^2 + c\eta_\mu^2 G^2 - 2\eta_\mu (d(\boldsymbol{\mu}_{k-1}) - P^*), \quad (34)$$

where (33) follows from the fact that $\Delta_{\boldsymbol{\mu}_{k-1}}$ is a subgradient of the dual function [38], leading to the inequality $(\boldsymbol{\mu}_{k-1} - \boldsymbol{\mu}^*)^T \mathbb{E} [\Delta_{\boldsymbol{\mu}_{k-1}} \mid \boldsymbol{\mu}_{k-1}] \geq d(\boldsymbol{\mu}_{k-1}) - d(\boldsymbol{\mu}^*)$ thanks to the dual function being convex [39]. Now, combining the fact that $\boldsymbol{\mu}_{k-1} \in \mathcal{C}^c$ with the definition of \mathcal{C} in (23), we can continue (34) as

$$\mathbb{E} [\|\boldsymbol{\mu}_k - \boldsymbol{\mu}^*\|^2 \mid \boldsymbol{\mu}_{k-1} \in \mathcal{C}^c] < \|\boldsymbol{\mu}_{k-1} - \boldsymbol{\mu}^*\|^2 \quad (35)$$

$$< \|\boldsymbol{\mu}_0 - \boldsymbol{\mu}^*\|^2, \quad (36)$$

with the last inequality following from recursion.

Proof of Compactness of \mathcal{A}_δ . Since the Minkowski sum of two compact sets is compact, and also the union of two compact sets is compact, it suffices to show that the set \mathcal{C} is compact.

Given the definition of the dual function in (22), for any set of model parameters $\boldsymbol{\theta} \in \Theta$ and any set of dual variables $\boldsymbol{\mu} \in \mathbb{R}_+^c$, we have

$$\begin{aligned} d(\boldsymbol{\mu}) & \geq \mathcal{U} \left(\frac{1}{T} \sum_{t=0}^{T-1} \mathbf{f}(\mathbf{H}_t, \mathbf{p}^\theta(\mathbf{H}_t; \boldsymbol{\theta})) \right) \\ & \quad + \boldsymbol{\mu}^T \mathbf{g} \left(\frac{1}{T} \sum_{t=0}^{T-1} \mathbf{f}(\mathbf{H}_t, \mathbf{p}^\theta(\mathbf{H}_t; \boldsymbol{\theta})) \right) \end{aligned} \quad (37)$$

Now, replacing $\boldsymbol{\theta}$ with the strictly-feasible set of model

parameters $\hat{\theta}$ considered in Theorem 1, we can write

$$d(\boldsymbol{\mu}) \geq \mathcal{U} \left(\frac{1}{T} \sum_{t=0}^{T-1} \mathbf{f}(\mathbf{H}_t, \mathbf{p}^\theta(\mathbf{H}_t; \hat{\theta})) \right) + \boldsymbol{\mu}^T \mathbf{g} \left(\frac{1}{T} \sum_{t=0}^{T-1} \mathbf{f}(\mathbf{H}_t, \mathbf{p}^\theta(\mathbf{H}_t; \hat{\theta})) \right) \quad (38)$$

$$\geq \mathcal{U} \left(\frac{1}{T} \sum_{t=0}^{T-1} \mathbf{f}(\mathbf{H}_t, \mathbf{p}^\theta(\mathbf{H}_t; \hat{\theta})) \right) + G' \|\boldsymbol{\mu}\|_1. \quad (39)$$

Now, for any $\boldsymbol{\mu} \in \mathcal{C}$, according to the definition in (23), the bound in (39) leads to

$$P^* + \frac{c\eta_\mu G^2}{2} \geq \mathcal{U} \left(\frac{1}{T} \sum_{t=0}^{T-1} \mathbf{f}(\mathbf{H}_t, \mathbf{p}^\theta(\mathbf{H}_t; \hat{\theta})) \right) + G' \|\boldsymbol{\mu}\|_1, \quad (40)$$

implying that $\boldsymbol{\mu}$ belongs to the following ball,

$$\|\boldsymbol{\mu}\|_1 \leq \frac{P^* + \frac{c\eta_\mu G^2}{2} - \mathcal{U} \left(\frac{1}{T} \sum_{t=0}^{T-1} \mathbf{f}(\mathbf{H}_t, \mathbf{p}^\theta(\mathbf{H}_t; \hat{\theta})) \right)}{G'}, \quad (41)$$

hence completing the proof. \square

B. Proof of Feasibility in (7)

From the dual dynamics in (6), we have

$$\boldsymbol{\mu}_K \geq \boldsymbol{\mu}_{K-1} - \eta_\mu \mathbf{g} \left(\frac{1}{T_0} \sum_{t=(K-1)T_0}^{KT_0-1} \mathbf{f}(\mathbf{H}_t, \mathbf{p}^\theta(\mathbf{H}_t; \boldsymbol{\theta}_{K-1})) \right). \quad (42)$$

Using the inequality in (42) recursively yields

$$\begin{aligned} \boldsymbol{\mu}_K &\geq \boldsymbol{\mu}_0 - \eta_\mu \sum_{k=0}^{K-1} \mathbf{g} \left(\frac{1}{T_0} \sum_{t=kT_0}^{(k+1)T_0-1} \mathbf{f}(\mathbf{H}_t, \mathbf{p}^\theta(\mathbf{H}_t; \boldsymbol{\theta}_k)) \right) \\ &= \boldsymbol{\mu}_0 - K\eta_\mu \cdot \frac{1}{K} \sum_{k=0}^{K-1} \mathbf{g} \left(\frac{1}{T_0} \sum_{t=kT_0}^{(k+1)T_0-1} \mathbf{f}(\mathbf{H}_t, \mathbf{p}^\theta(\mathbf{H}_t; \boldsymbol{\theta}_k)) \right) \\ &\geq \boldsymbol{\mu}_0 - K\eta_\mu \mathbf{g} \left(\frac{1}{KT_0} \sum_{t=0}^{KT_0-1} \mathbf{f}(\mathbf{H}_t, \mathbf{p}^\theta(\mathbf{H}_t; \boldsymbol{\theta}_{\lfloor t/T_0 \rfloor}) \right), \end{aligned}$$

where the last inequality follows from the concavity of $\mathbf{g}(\cdot)$. Therefore, we have

$$\begin{aligned} \limsup_{K \rightarrow \infty} \boldsymbol{\mu}_{K+1} &\geq \boldsymbol{\mu}_0 - \eta_\mu \liminf_{K \rightarrow \infty} K \mathbf{g} \left(\frac{1}{T} \sum_{t=0}^{T-1} \mathbf{f}(\mathbf{H}_t, \mathbf{p}^\theta(\mathbf{H}_t; \boldsymbol{\theta}_{\lfloor t/T_0 \rfloor}) \right). \end{aligned} \quad (43)$$

Now, assume by contradiction that one of the constraints in (7) is not satisfied. More precisely, assume there exists an index $i \in \{1, \dots, c\}$ and positive constants $\delta > 0$ and $\beta \in (0, 1)$

such that

$$\Pr \left[\liminf_{T \rightarrow \infty} g_i \left(\frac{1}{T} \sum_{t=0}^{T-1} \mathbf{f}(\mathbf{H}_t, \mathbf{p}^\theta(\mathbf{H}_t; \boldsymbol{\theta}_{\lfloor t/T_0 \rfloor}) \right) \leq -\delta \right] = \beta. \quad (44)$$

This implies that with non-zero probability β , we would have

$$\begin{aligned} \limsup_{K \rightarrow \infty} \|\boldsymbol{\mu}_K\|_1 &\geq \limsup_{K \rightarrow \infty} \mu_{i,K} \end{aligned} \quad (45)$$

$$\geq \mu_{i,0} - \eta_\mu \liminf_{K \rightarrow \infty} K g_i \left(\frac{1}{T} \sum_{t=0}^{T-1} \mathbf{f}(\mathbf{H}_t, \mathbf{p}^\theta(\mathbf{H}_t; \boldsymbol{\theta}_{\lfloor t/T_0 \rfloor}) \right) \quad (46)$$

$$\geq \mu_{i,0} + \eta_\mu \liminf_{K \rightarrow \infty} K \epsilon \quad (47)$$

$$= \infty, \quad (48)$$

where (45) follows from the definition of the ℓ_1 -norm, (46) follows from the i^{th} inequality in (43), and (47) follows from (44). This contradicts the fact that the sequence of dual variable probabilities is tight, hence completing the proof. \square

C. Proof of Optimality in (8)

Given the dual dynamics in (6) and the fact that projection onto the non-negative orthant does not increase the ℓ_2 -norm, we have

$$\begin{aligned} \|\boldsymbol{\mu}_{K+1}\|^2 &\leq \left\| \boldsymbol{\mu}_K - \eta_\mu \mathbf{g} \left(\frac{1}{T_0} \sum_{t=KT_0}^{(K+1)T_0-1} \mathbf{f}(\mathbf{H}_t, \mathbf{p}^\theta(\mathbf{H}_t; \boldsymbol{\theta}_K)) \right) \right\|^2 \end{aligned} \quad (49)$$

$$\begin{aligned} &= \|\boldsymbol{\mu}_K\|^2 + \eta_\mu^2 \left\| \mathbf{g} \left(\frac{1}{T_0} \sum_{t=KT_0}^{(K+1)T_0-1} \mathbf{f}(\mathbf{H}_t, \mathbf{p}^\theta(\mathbf{H}_t; \boldsymbol{\theta}_K)) \right) \right\|^2 \\ &\quad - 2\eta_\mu \boldsymbol{\mu}_K^T \mathbf{g} \left(\frac{1}{T_0} \sum_{t=KT_0}^{(K+1)T_0-1} \mathbf{f}(\mathbf{H}_t, \mathbf{p}^\theta(\mathbf{H}_t; \boldsymbol{\theta}_K)) \right) \quad (50) \\ &\leq \|\boldsymbol{\mu}_T\|^2 + c\eta_\mu^2 G^2 \\ &\quad - 2\eta_\mu \boldsymbol{\mu}_K^T \mathbf{g} \left(\frac{1}{T_0} \sum_{t=KT_0}^{(K+1)T_0-1} \mathbf{f}(\mathbf{H}_t, \mathbf{p}^\theta(\mathbf{H}_t; \boldsymbol{\theta}_K)) \right), \end{aligned} \quad (51)$$

where the last inequality follows from the fact that for any $i \in \{1, \dots, c\}$, we assume $|g_i(\cdot)| \leq G$. Applying (51) recursively yields

$$\begin{aligned} \|\boldsymbol{\mu}_{K+1}\|^2 &\leq \|\boldsymbol{\mu}_0\|^2 + c\eta_\mu^2 K G^2 \\ &\quad - 2\eta_\mu \sum_{k=0}^{K-1} \boldsymbol{\mu}_k^T \mathbf{g} \left(\frac{1}{T_0} \sum_{t=kT_0}^{(k+1)T_0-1} \mathbf{f}(\mathbf{H}_t, \mathbf{p}^\theta(\mathbf{H}_t; \boldsymbol{\theta}_k)) \right). \end{aligned} \quad (52)$$

Since $\|\boldsymbol{\mu}_{K+1}\|^2 \geq 0$, rearranging the terms in (52) and normalizing both sides by $2\eta\boldsymbol{\mu}K$ results in

$$\begin{aligned} & \frac{1}{K} \sum_{k=0}^{K-1} \boldsymbol{\mu}_k^T \mathbf{g} \left(\frac{1}{T_0} \sum_{t=kT_0}^{(k+1)T_0-1} \mathbf{f}(\mathbf{H}_t, \mathbf{p}^\theta(\mathbf{H}_t; \boldsymbol{\theta}_k)) \right) \\ & \leq \frac{1}{2\eta\boldsymbol{\mu}K} \|\boldsymbol{\mu}_0\|^2 + \frac{c\eta\boldsymbol{\mu}G^2}{2}. \end{aligned} \quad (53)$$

Taking the conditional expectation of both sides in (53) given $\boldsymbol{\mu}_0$, and letting $K \rightarrow \infty$, we can write

$$\begin{aligned} & \limsup_{K \rightarrow \infty} \mathbb{E} \left[\sum_{k=0}^{K-1} \frac{\boldsymbol{\mu}_k^T}{K} \mathbf{g} \left(\frac{1}{T_0} \sum_{t=kT_0}^{(k+1)T_0-1} \frac{\mathbf{f}(\mathbf{H}_t, \mathbf{p}^\theta(\mathbf{H}_t; \boldsymbol{\theta}_k))}{T_0} \right) \middle| \boldsymbol{\mu}_0 \right] \\ & \leq \frac{c\eta\boldsymbol{\mu}G^2}{2}. \end{aligned} \quad (54)$$

For any iteration k , since $\boldsymbol{\theta}_k$ is the maximizer of (5), for any $\boldsymbol{\theta} \in \Theta$, we can write

$$\begin{aligned} & \mathcal{U} \left(\frac{1}{T_0} \sum_{t=kT_0}^{(k+1)T_0-1} \mathbf{f}(\mathbf{H}_t, \mathbf{p}^\theta(\mathbf{H}_t; \boldsymbol{\theta}_k)) \right) \\ & \quad + \boldsymbol{\mu}_k^T \mathbf{g} \left(\frac{1}{T_0} \sum_{t=kT_0}^{(k+1)T_0-1} \mathbf{f}(\mathbf{H}_t, \mathbf{p}^\theta(\mathbf{H}_t; \boldsymbol{\theta}_k)) \right) \\ & \geq \mathcal{U} \left(\frac{1}{T_0} \sum_{t=kT_0}^{(k+1)T_0-1} \mathbf{f}(\mathbf{H}_t, \mathbf{p}^\theta(\mathbf{H}_t; \boldsymbol{\theta})) \right) \\ & \quad + \boldsymbol{\mu}_k^T \mathbf{g} \left(\frac{1}{T_0} \sum_{t=kT_0}^{(k+1)T_0-1} \mathbf{f}(\mathbf{H}_t, \mathbf{p}^\theta(\mathbf{H}_t; \boldsymbol{\theta})) \right) \end{aligned}$$

Taking the expectations of both sides conditioned on $\boldsymbol{\mu}_k$, we have

$$\begin{aligned} & \mathbb{E} \left[\mathcal{U} \left(\frac{1}{T_0} \sum_{t=kT_0}^{(k+1)T_0-1} \mathbf{f}(\mathbf{H}_t, \mathbf{p}^\theta(\mathbf{H}_t; \boldsymbol{\theta}_k)) \right) \middle| \boldsymbol{\mu}_k \right] \\ & \quad + \boldsymbol{\mu}_k^T \mathbb{E} \left[\mathbf{g} \left(\frac{1}{T_0} \sum_{t=kT_0}^{(k+1)T_0-1} \mathbf{f}(\mathbf{H}_t, \mathbf{p}^\theta(\mathbf{H}_t; \boldsymbol{\theta}_k)) \right) \middle| \boldsymbol{\mu}_k \right] \\ & \geq \mathbb{E} \left[\mathcal{U} \left(\frac{1}{T_0} \sum_{t=kT_0}^{(k+1)T_0-1} \mathbf{f}(\mathbf{H}_t, \mathbf{p}^\theta(\mathbf{H}_t; \boldsymbol{\theta})) \right) \right] \\ & \quad + \boldsymbol{\mu}_k^T \mathbb{E} \left[\mathbf{g} \left(\frac{1}{T_0} \sum_{t=kT_0}^{(k+1)T_0-1} \mathbf{f}(\mathbf{H}_t, \mathbf{p}^\theta(\mathbf{H}_t; \boldsymbol{\theta})) \right) \right] \quad (55) \\ & = \mathbb{E} \left[\mathcal{U} \left(\frac{1}{T_0} \sum_{t=kT_0}^{(k+1)T_0-1} \mathbf{f}(\mathbf{H}_t, \mathbf{p}^\theta(\mathbf{H}_t; \boldsymbol{\theta})) \right) \right] \\ & \quad + \underbrace{\boldsymbol{\mu}_k^T \mathbb{E} \left[\mathbf{g} \left(\frac{1}{T_0} \sum_{t=kT_0}^{(k+1)T_0-1} \mathbf{f}(\mathbf{H}_t, \mathbf{p}^\theta(\mathbf{H}_t; \boldsymbol{\theta})) \right) \right]}_{\geq 0 \text{ for any feasible } \boldsymbol{\theta} \in \Theta} \end{aligned} \quad (56)$$

$$\begin{aligned} & = \lim_{T \rightarrow \infty} \mathcal{U} \left(\frac{1}{T} \sum_{t=0}^{T-1} \mathbf{f}(\mathbf{H}_t, \mathbf{p}^\theta(\mathbf{H}_t; \boldsymbol{\theta})) \right) \\ & \quad + \underbrace{\boldsymbol{\mu}_k^T \lim_{T \rightarrow \infty} \mathbf{g} \left(\frac{1}{T} \sum_{t=0}^{T-1} \mathbf{f}(\mathbf{H}_t, \mathbf{p}^\theta(\mathbf{H}_t; \boldsymbol{\theta})) \right)}_{\geq 0 \text{ for any feasible } \boldsymbol{\theta} \in \Theta} \end{aligned} \quad (57)$$

$$\geq \lim_{T \rightarrow \infty} \mathcal{U} \left(\frac{1}{T} \sum_{t=0}^{T-1} \mathbf{f}(\mathbf{H}_t, \mathbf{p}^\theta(\mathbf{H}_t; \boldsymbol{\theta})) \right), \quad (58)$$

where (57) follows from the fact that the expected value of the utility and the constraints within each iteration provide unbiased estimates of the objective and constraints in (2), respectively; i.e., for any $k \in \{0, 1, 2, \dots, K-1\}$ and $\forall \boldsymbol{\theta} \in \Theta$,

$$\begin{aligned} & \mathbb{E} \left[\mathcal{U} \left(\frac{1}{T_0} \sum_{t=kT_0}^{(k+1)T_0-1} \mathbf{f}(\mathbf{H}_t, \mathbf{p}^\theta(\mathbf{H}_t; \boldsymbol{\theta})) \right) \right] \\ & = \lim_{T \rightarrow \infty} \mathcal{U} \left(\frac{1}{T} \sum_{t=0}^{T-1} \mathbf{f}(\mathbf{H}_t, \mathbf{p}^\theta(\mathbf{H}_t; \boldsymbol{\theta})) \right) \quad (59) \\ & \mathbb{E} \left[\mathbf{g} \left(\frac{1}{T_0} \sum_{t=kT_0}^{(k+1)T_0-1} \mathbf{f}(\mathbf{H}_t, \mathbf{p}^\theta(\mathbf{H}_t; \boldsymbol{\theta})) \right) \right] \\ & = \lim_{T \rightarrow \infty} \mathbf{g} \left(\frac{1}{T} \sum_{t=0}^{T-1} \mathbf{f}(\mathbf{H}_t, \mathbf{p}^\theta(\mathbf{H}_t; \boldsymbol{\theta})) \right). \quad (60) \end{aligned}$$

The inequality in (58) is true for all feasible $\boldsymbol{\theta} \in \Theta$, especially for the optimal set of parameters $\boldsymbol{\theta}^*$, for which the RHS of (58) equals P^* . Therefore, we have

$$\begin{aligned} & \mathbb{E} \left[\mathcal{U} \left(\frac{1}{T_0} \sum_{t=kT_0}^{(k+1)T_0-1} \mathbf{f}(\mathbf{H}_t, \mathbf{p}^\theta(\mathbf{H}_t; \boldsymbol{\theta}_k)) \right) \middle| \boldsymbol{\mu}_k \right] \\ & \geq P^* - \boldsymbol{\mu}_k^T \mathbb{E} \left[\mathbf{g} \left(\frac{1}{T_0} \sum_{t=kT_0}^{(k+1)T_0-1} \mathbf{f}(\mathbf{H}_t, \mathbf{p}^\theta(\mathbf{H}_t; \boldsymbol{\theta}_k)) \right) \middle| \boldsymbol{\mu}_k \right]. \end{aligned} \quad (61)$$

Averaging the above inequality over $k \in \{0, \dots, K-1\}$, and taking the expected value conditioned on $\boldsymbol{\mu}_0$, we will get

$$\begin{aligned} & \mathbb{E} \left[\frac{1}{K} \sum_{k=0}^{K-1} \mathcal{U} \left(\frac{1}{T_0} \sum_{t=kT_0}^{(k+1)T_0-1} \mathbf{f}(\mathbf{H}_t, \mathbf{p}^\theta(\mathbf{H}_t; \boldsymbol{\theta}_k)) \right) \middle| \boldsymbol{\mu}_0 \right] \\ & \geq P^* \\ & \quad - \mathbb{E} \left[\frac{1}{K} \sum_{k=0}^{K-1} \boldsymbol{\mu}_k^T \mathbf{g} \left(\frac{1}{T_0} \sum_{t=kT_0}^{(k+1)T_0-1} \mathbf{f}(\mathbf{H}_t, \mathbf{p}^\theta(\mathbf{H}_t; \boldsymbol{\theta}_k)) \right) \middle| \boldsymbol{\mu}_0 \right]. \end{aligned} \quad (62)$$

Letting $K \rightarrow \infty$, and plugging (54) into (62), we have

$$\begin{aligned} & P^* - \frac{c\eta\boldsymbol{\mu}G^2}{2} \\ & \leq P^* \\ & \quad - \limsup_{K \rightarrow \infty} \mathbb{E} \left[\sum_{k=0}^{K-1} \frac{\boldsymbol{\mu}_k^T}{K} \mathbf{g} \left(\frac{1}{T_0} \sum_{t=kT_0}^{(k+1)T_0-1} \frac{\mathbf{f}(\mathbf{H}_t, \mathbf{p}^\theta(\mathbf{H}_t; \boldsymbol{\theta}_k))}{T_0} \right) \middle| \boldsymbol{\mu}_0 \right] \end{aligned} \quad (63)$$

$$\leq \liminf_{K \rightarrow \infty} \mathbb{E} \left[\frac{1}{K} \sum_{k=0}^{K-1} \mathcal{U} \left(\frac{1}{T_0} \sum_{t=kT_0}^{(k+1)T_0-1} \mathbf{f}(\mathbf{H}_t, \mathbf{p}^\theta(\mathbf{H}_t; \boldsymbol{\theta}_k)) \right) \right] \quad (64)$$

$$\leq \liminf_{K \rightarrow \infty} \mathbb{E} \left[\mathcal{U} \left(\frac{1}{K} \sum_{k=0}^{K-1} \frac{1}{T_0} \sum_{t=kT_0}^{(k+1)T_0-1} \mathbf{f}(\mathbf{H}_t, \mathbf{p}^\theta(\mathbf{H}_t; \boldsymbol{\theta}_k)) \right) \right] \quad (65)$$

$$= \liminf_{T \rightarrow \infty} \mathbb{E} \left[\mathcal{U} \left(\frac{1}{T} \sum_{t=0}^{T-1} \mathbf{f}(\mathbf{H}_t, \mathbf{p}^\theta(\mathbf{H}_t; \boldsymbol{\theta}_{\lfloor t/T_0 \rfloor}) \right) \right] \quad (66)$$

where (65) is due to concavity of \mathcal{U} . This completes the proof, due to the assumption that the limit on the left-hand side of (66) exists. \square

APPENDIX B PROOF OF THEOREM 2

The proof of feasibility in (15) follows similar steps to those in Appendix A-B and we, therefore, omit it for brevity. As for the near-optimality result in (16), we have

$$\begin{aligned} & \lim_{T \rightarrow \infty} \left| \mathbb{E} \left[\mathcal{U} \left(\frac{1}{T} \sum_{t=0}^{T-1} \mathbf{f}(\mathbf{H}_t, \mathbf{p}^\phi(\mathbf{H}_t, \boldsymbol{\mu}_{\lfloor t/T_0 \rfloor}; \boldsymbol{\phi}^*)) \right) \right. \right. \\ & \quad \left. \left. - \mathcal{U} \left(\frac{1}{T} \sum_{t=0}^{T-1} \mathbf{f}(\mathbf{H}_t, \mathbf{p}^\theta(\mathbf{H}_t; \boldsymbol{\theta}_{\lfloor t/T_0 \rfloor}) \right) \right) \right] \right| \quad (67) \\ & \leq \lim_{T \rightarrow \infty} \mathbb{E} \left| \mathcal{U} \left(\frac{1}{T} \sum_{t=0}^{T-1} \mathbf{f}(\mathbf{H}_t, \mathbf{p}^\phi(\mathbf{H}_t, \boldsymbol{\mu}_{\lfloor t/T_0 \rfloor}; \boldsymbol{\phi}^*)) \right) \right. \end{aligned}$$

$$\left. - \mathcal{U} \left(\frac{1}{T} \sum_{t=0}^{T-1} \mathbf{f}(\mathbf{H}_t, \mathbf{p}^\theta(\mathbf{H}_t; \boldsymbol{\theta}_{\lfloor t/T_0 \rfloor}) \right) \right| \quad (68)$$

$$\leq \lim_{T \rightarrow \infty} \mathbb{E} \left\| \frac{1}{T} \sum_{t=0}^{T-1} \left(\mathbf{f}(\mathbf{H}_t, \mathbf{p}^\phi(\mathbf{H}_t, \boldsymbol{\mu}_{\lfloor t/T_0 \rfloor}; \boldsymbol{\phi}^*)) - \mathbf{f}(\mathbf{H}_t, \mathbf{p}^\theta(\mathbf{H}_t; \boldsymbol{\theta}_{\lfloor t/T_0 \rfloor}) \right) \right\|_\infty \quad (69)$$

$$\leq \lim_{T \rightarrow \infty} \frac{1}{T} \sum_{t=0}^{T-1} \mathbb{E} \left\| \mathbf{f}(\mathbf{H}_t, \mathbf{p}^\phi(\mathbf{H}_t, \boldsymbol{\mu}_{\lfloor t/T_0 \rfloor}; \boldsymbol{\phi}^*)) - \mathbf{f}(\mathbf{H}_t, \mathbf{p}^\theta(\mathbf{H}_t; \boldsymbol{\theta}_{\lfloor t/T_0 \rfloor}) \right\|_\infty \quad (70)$$

$$\leq M \lim_{T \rightarrow \infty} \frac{1}{T} \sum_{t=0}^{T-1} \mathbb{E} \left\| \mathbf{p}^\phi(\mathbf{H}_t, \boldsymbol{\mu}_{\lfloor t/T_0 \rfloor}; \boldsymbol{\phi}^*) - \mathbf{p}^\theta(\mathbf{H}_t; \boldsymbol{\theta}_{\lfloor t/T_0 \rfloor}) \right\|_\infty \quad (71)$$

$$\leq M \mathbb{E} \left\| \mathbf{p}^\phi(\mathbf{H}, \boldsymbol{\mu}; \boldsymbol{\phi}^*) - \mathbf{p}^\theta(\mathbf{H}; \boldsymbol{\theta}(\boldsymbol{\mu})) \right\|_\infty \quad (72)$$

$$\leq M\epsilon, \quad (73)$$

where (68) results from the convexity of the absolute value function, (69) comes from the Lipschitz continuity of the utility \mathcal{U} , (70) results from the convexity of the ℓ_∞ norm, (71) holds because of the Lipschitz continuity of the performance function \mathbf{f} , (72) holds since $\{\boldsymbol{\mu}_k\}_{k=1}^K$ are assumed to come from the distribution p_μ , and (73) is true due to the near-universality of the parameterization. This, combined with (8) from Theorem 1, completes the proof. \square